Modelling the collective response of heterogeneous cell populations to stationary gradients and chemical signal relay

Pineda, Miguel ; Eftimie, Raluca

Published in:
Physical Biology

DOI:
10.1088/1478-3975/aa89b4

Publication date:
2017

Physical Biology

OFFICIAL JOURNAL OF
Sociedad de Biofísicos Latino Americanos

Modelling the collective response of heterogeneous cell populations to stationary gradients and chemical signal relay

To cite this article before publication: Miguel Pineda *et al* 2017 *Phys. Biol.* in press https://doi.org/10.1088/1478-3975/aa89b4

Modelling the collective response of heterogeneous cell populations to stationary gradients and chemical signal relay.

M Pineda[1] and R Eftimie[2]

[1]Department of Chemical Engineering, University College London, Roberts Building, Torrington Place, London WC1E 7JE, United Kingdom

[2]Division of Mathematics, University of Dundee, Dundee DD1 4HN, United Kingdom

E-mail: [1]m.pineda@ucl.ac.uk

E-mail: [2]reftimie@maths.dundee.ac.uk

Abstract. The directed motion of cell aggregates toward a chemical source occurs in many relevant biological processes. Understanding the mechanisms that control this complex behavior is of great relevance for our understanding of developmental biological processes and many diseases. In this paper, we consider a self-propelled particle model for the movement of heterogeneous subpopulations of chemically interacting cells towards an imposed stable chemical gradient. Our simulations show explicitly how self-organisation of cell populations (which could lead to engulfment or complete cell segregation) can arise from the heterogeneity of chemotactic responses alone. This new result complements current theoretical and experimental studies that emphasise the role of differential cell-cell adhesion on self-organisation and spatial structure of cellular aggregates. We also investigate how the speed of individual cell aggregations increases with the chemotactic sensitivity of the cells, and decreases with the number of cells inside the aggregates.

1. Introduction

Long-distance collective migration of cells is a biological process important for the establishment and maintenance of multicellular organisms. This orchestrated movement is vital during wound healing, embryonic development and immune responses. Defects during this collective behavior of cells can result in serious health problems, including vascular diseases, tumor formation, and cancer metastasis. These are some of the reasons why the study of the mechanisms by which a population of cells migrate in a coordinated manner is of extreme importance for better understanding many birth defects and diseases [1, 2, 3].

It is well known that many types of cells respond to chemotactic signals that drive the collective motion of individual cells or cellular aggregates [4, 5, 6]. Cell

chemotaxis has been the subject of intense study during the past years, and thus many details related to the response of individual cells to chemicals are currently known [7]. However, the response of a collective of interacting cells to chemical signals is poorly understood [8]. The complexity of the problem is enhanced by the fact that in many cases these aggregates are composed of different subpopulations of cells having different chemotactic responses, and therefore, different motility properties.

In developmental biology, two of the most studied examples of collective chemotactic behavior in different subpopulations of cells are related to the motion of the multicellular microorganism *Dictyostelium discoideum*, and the motion of neural crest (NC) cells [9, 10, 11, 12]. In regard to the *Dictyostelium discoideum* cells, their different stages of development are characterized by the cooperative motion of two main types of cells (prestalk and prespore cells) with different chemotactic and mobility properties. Systematic experiments of chemotactic behavior under adjustable and controlled conditions have been performed in order to study the response of groups of *Dictyostelium discoideum* cells to temporally stable gradients of $3'$,$5'$-cyclic adenosine monophosphate (cAMP) [13, 14, 15]. Although many experimental studies removed any chemicals released by the cells themselves, few others considered the interplay between the relay of self-produced cAMP signals and cells response towards stable external cAMP gradients [15]. These studies have been complemented by various theoretical approaches, most of which consider homogeneous groups of cells with similar general properties (e.g., same chemotactic responses and same cell speeds) [14, 15]. However, as mentioned above, in many cases collective cell movement is the result of interactions among heterogeneous cell populations with different signal sensing and signal relay capabilities (see *Dictyostelium discoideum* development that involves prespore and prestalk cells [12]). Similar experiments have been used to analyze the response to chemical gradients of neutrophils [16], cancer cells [17], and bacteria [18].

During embryonic development, different NC cells with different chemotactic responses migrate ventrally through the embryo, guided by migratory pathways [10, 11]. Chemotactic interaction between cells is also a very common phenomenon in different physiological contexts. For example, wound healing in the corneal epithelium is determined by the migration into the wound of interacting sub-aggregates of epithelial cells [19], while during tumor progression mutated cells move through and interact with different populations of healthy and immune cells [20].

In this work, we present a general particle model derived to investigate how a mixture of heterogeneous interacting cell populations, which produce, relay and degrade a chemical signal, respond to an external stable gradient of a different chemical signal [21], and form various aggregation patterns. In our model the cells are represented as self-propelled particles (SPP) that behave as soft disks [22, 23]. We show how

the response of the two populations to the external chemical gradient is determined by the chemotactic sensitivity of the cells, the mutual mechanical interaction between cells, and the overall chemical signal degradation rate [24, 25]. **Our computational simulations show how self-organisation of cell populations (which could lead to engulfment or complete cell segregation) can arise from the heterogeneity of chemotactic responses alone. These results complement current studies that emphasise the role of differential cell-cell adhesion on self-organisation and spatial structure of cellular aggregates [26, 27].** Although this work is inspired by previous studies concerning the response of *Dictyostelium discoideum* cells to external gradients [15], its novelty lies in the investigation of the interactions between multiple heterogeneous cell populations, and in the investigation of the importance of mechanical vs. chemotactic interactions on collective cell migration and aggregation.

This paper is organized as follows. In Sec. 2, we introduce the general SPP model implemented in this work. In Sec. 3, we analyze how two groups of mechanical and chemotactic interacting cells, with different chemotactic coefficients and/or average cell speeds, respond to an external stable chemical signal. In particular, we discuss how the relevant parameters of the model affect the response of the cells to different chemical gradient steepness. To this end, we introduce an order parameter that quantifies the global alignment of cells, and we investigate the changes in this order parameter as we vary different control parameters of the model. We also explore how the velocity of single cell aggregations changes with the number of cells and the chemotactic sensitivity. Finally, in Sec. 4 we present our summary and conclusions.

2. The self-propelled particle model

We describe a group of N cells as a self-propelled particle system, in which each cell behaves as a soft disk of radius $r_0 = 0.0075$ mm. The kinetics of the system occurs in a two-dimensional impermeable $L_x \times L_y$ rectangular domain inside which the state of cell i at time t is characterized by its location vector $\vec{r}_i(x, y, t)$ and by the direction $\theta_i(t)$ of its velocity vector $\vec{v}_i(t)$. In agreement with controlled chemotaxis experiments [28, 29], the speed $\|\vec{v}_i(t)\|$ of each cell is assumed to have a constant value ν_i. Then, the updated position of the ith cell is expressed as [7, 22, 23, 15]:

$$\vec{r}_i(x, y, t + \Delta t) = \vec{r}_i(x, y, t) + \Delta t \vec{v}_i(t), \tag{1}$$

with

$$\vec{v}_i(t) = \nu_i \vec{e}_i(t) = \nu_i \begin{pmatrix} \cos\theta_i(t) \\ \sin\theta_i(t) \end{pmatrix}, \tag{2}$$

and

$$\theta_i(t + \Delta t) = arg \left\{ \chi_i \frac{\vec{\nabla} C_T(t)}{\|\vec{\nabla} C_T(t)\|} + \sum_{\substack{j=1 \\ i \neq j}}^{N} m_{ij} \vec{F}_{ij}(t) + \alpha_i \vec{\sigma}_i(t) \right\}. \tag{3}$$

In Eq. (2) the unit vector $\vec{e}_i$ gives the direction along which a single cell moves. The first term in Eq. (3) represents a unitary vector pointing in the direction of increased chemical signal concentration (C_T), multiplied by the chemotaxis sensitivity χ_i. Normally, it is assumed that χ_i decreases nonlinearly with C_T [30, 31, 32]. However, according to the experimental results that motivated this work [15], we will assume that this term is independent of the level of the chemical signal. Note that arg gives the angle of the resulting vector.

In our model the total chemical signal C_T is originated from two sources: the single cells that secrete a local chemical signal C_I into the extracellular space, and an externally imposed stable gradient of a different chemical C_E which is changing only along the y direction. We consider that $C_T = C_I + C_E$ or $\vec{\nabla} C_T = \vec{\nabla} C_I + \vec{\nabla} C_E$. After assuming that secretion, degradation, and diffusion of C_I are much faster than all other processes of the model, the chemical gradient generated by the cells can be written as

$$\vec{\nabla} C_I(\vec{r_i}) = -p \sum_{j \neq i}^{N} K_1(\|\vec{r_i} - \vec{r_j}\|/\ell)\vec{r}_{ij}, \tag{4}$$

where K_1 is a modified Bessel function of the second kind, $\ell = \sqrt{D_I/\mu_I}$, and p quantifies the response of the cells to the chemical gradient. The sum is over the simulated cells other than cell i. The vector $\vec{r}_{ij}$ is a unitary vector directed from j to i. The parameters D_I and μ_I are the constant chemical diffusivity and chemical signal degradation rate, respectively [33]. Note that the parameter N is the total number of cells and the local chemical signal is secreted at every position r_i of cells.

We assume that the external chemical signal only changes along the y directions and its dynamics is governed by

$$\frac{\partial C_E}{\partial t} = D_E \vec{\nabla}^2 C_E - \mu_E C_E, \tag{5}$$

with boundary conditions along the y direction: $C_E(y = 0) = 0$ and $C_E(y = L_y) = C_m$. **As in [15], we choose fixed-concentration boundary conditions to describe the case where the external chemical is applied only at the upper boundary of the domain.** Assuming also steady state conditions (since the dynamics of the chemical is much faster than all other processes in the model), one obtains

$$C_E(y) = C_m \frac{e^{-\sqrt{\frac{\mu_E}{D_E}}y} - e^{\sqrt{\frac{\mu_E}{D_E}}y}}{e^{-\sqrt{\frac{\mu_E}{D_E}}L_y} - e^{\sqrt{\frac{\mu_E}{D_E}}L_y}}, \tag{6}$$

with the corresponding gradient given by

$$\vec{\nabla} C_E(y) = -C_m \sqrt{\frac{\mu_E}{D_E}} \frac{e^{-\sqrt{\frac{\mu_E}{D_E}}y} + e^{\sqrt{\frac{\mu_E}{D_E}}y}}{e^{-\sqrt{\frac{\mu_E}{D_E}}L_y} - e^{\sqrt{\frac{\mu_E}{D_E}}L_y}} \hat{\mathbf{y}}, \tag{7}$$

where $\hat{\mathbf{y}}$ is a unitary vector point in the y direction. **Note that the gradient of the external chemical described in Eq. (7) depends on the concentration C_m at the upper boundary of the domain. In supplemental material we plot Eq. (6) (external chemical profile) as a function of L_y (Fig. S1A) and μ_E (Fig.**

S1B). Figure S1A shows that the chemical profile substantially increases near the upper edge of the domain where $C_E(y = L_y) = C_m$. However, Fig. S1B reveals that the steepness of such a profile decreases with the chemical degradation rate μ_E. In particular, it shows that for small enough values of the degradation rate the external chemical profile may extend along the whole domain.

The second term in Eq. (3) is responsible for the repulsive soft mutual interaction between cells [34, 35]. To describe it, let us consider a cell i. A second cell j exerts a repulsive force $\vec{F}_{ij}(t) = f_{ij}(t)\vec{r}_{ij}(t)$ upon cell i. The vector $\vec{r}_{ij}$ is a unitary vector directed from j to i, and $f_{ij}(t)$ is defined as

$$f_{ij} = \begin{cases} 0 & \text{if } r_{ij}(t) > 2r_o, \\ 1 - \frac{r_{ij}(t)}{2r_0} & \text{if } 0 \leq r_{ij}(t) \leq 2r_o, \end{cases}$$

where $r_{ij}(t) = \|\vec{r}_i(x, y, t) - \vec{r}_j(x, y, t)\|$ is the distance between cells. The repulsive force decreases linearly with distance from the center of the cell, and it is zero for $r_{ij}(t) > 2r_o$ (where we define $2r_o$ to be the interaction radius between two cells). The parameter m_{ij} that appears in Eq. (3) controls the intensity of the repulsive cell-cell interactions.

The last term in Eq. (3) is described by $\vec{\sigma}_i = (\cos\zeta_i(t), \sin\zeta_i(t))$, a random uniformly oriented unitary vector, multiplied by parameter α_i, which quantifies the noise intensity. The variable $\zeta_i(t)$ is a random number drawn between 0 and 2π.

Finally, in this work we assume for simplicity that the chemical diffusivity and degradation rate are the same for both the local and external chemicals: $\mu_I = \mu_E = \mu$ and $D_I = D_E = D$. However, the response of the cells to the local chemical signal is distinguished from the response to the external chemical gradient by the parameter p. We also assume that $m_{ij} = m_c$ and $\alpha_i = \alpha \; \forall \, i, j$. With these assumptions in mind, we present the results of our study in the following section.

3. Results

As mentioned above, in this work we investigate how heterogeneous interacting cell subpopulations with distinct motility properties react towards externally imposed chemical signals. To achieve this, we divide the group of N cells into subpopulations A and B [24, 25]. For simplicity, let us also assume that both subpopulation have the same number of cells ($N_A = N_B = N/2$), and that cells inside each subpopulation exhibit the same mechanical and chemotactic properties. However, given that the subpopulations may differ in cell speed and/or chemotactic sensitivity, we consider each cell i of type A or B (where cells A have lower speeds and/or chemotactic sensitivities compared to cells B).

Then, the system is iterated in time with a time step $\Delta t = 2 \times 10^{-2}$ min. To be in line with the experiments of Guven *et. al.* [15] in which a uniform cell injection flux is considered (with the orientation of each newly introduced cell assumed to be initially in the y direction), we simulated Eq. (1) with all cells starting at $y = 0$, uniformly

distributed along x axis and oriented only in the y direction. However, after this initial step, the cells can change their orientation (in response to the chemical signal, the social forces, and randomly). Then, we proceed to characterize the collective motion of cells by the order parameter M defined as in [36, 37, 38]:

$$M = \frac{1}{N} \left\| \sum_{i=1}^{N} \vec{e}_i(t) \right\|. \tag{8}$$

This order parameter runs from 0 to 1 and measures the degree of alignment of the cells. It is approximately zero if the direction of the individual cells is distributed randomly, while for a coherent cell motion $M \approx 1$. Given that at time $t = 0$ all cells are aligned towards the y direction, the order parameter is in this case $M = 1$. To avoid any artifact induced by the collision of the cells with the upper wall of the domain in which $C_E(y = L_y) = C_m$, all simulation results are obtained before the cells reach that wall. (Note that in the experimental results reported by Guven *et. al.* [15], the cells were removed after they reached the upper wall of the domain.)

In the following section we start exploring the collective alignment of the model when the two groups differ only in their chemotactic sensitivity. Then, we consider the case in which the groups differ in chemotactic sensitivity and cell speed. In the last subsection, we investigate how the speed of a single cell aggregation changes with relevant control parameters.

3.1. Two groups of cells with different chemotactic sensitivity.

In this section we consider the case in which the two groups of cells exhibit different chemotactic sensitivities: each cell i belonging to the group A reacts to the chemical signals with a chemoattractive sensitivity of $\chi_i = \chi_i^A = 0.75$, while any cell i of the second group B possesses a stronger chemotactive sensitivity of $\chi_i = \chi_i^B = 1.5$. The speed of each of the N cells is given by $\nu_i = \nu_o + \epsilon g_i$, where $\nu_o = 0.005$ mm min^{-1} is the average speed over all cells and g_i is an nondimensional number drawn from a Gaussian distribution with zero mean and unit variance. The constant parameter ϵ is small and given by 10^{-4} mm min^{-1}. This noise term considers the heterogeneities in individual cell speeds that are always present in many multicellular system. In the following, we investigate how the collective cell migration is affected by the dimension of the domain and the competition between different external gradient steepness (i.e., variations of C_m) and variations of p and μ.

First, let us to study the impact of the size of the domain (parameters L_x and L_y) on the collective dynamics of the system. To this end, in Fig. 1(A) we plot the order parameter M as a function of p, for three values of L_y, with $L_x = 0.75$ mm. To avoid collisions between the cells and the upper wall, the maximum simulation time is fixed at $t = 200$ min. Note that, at $t = 200$ min, any cell starting at $y = 0$ mm and moving all the time towards the y direction with a speed of $\nu_o = 0.005$ mm min^{-1} will be at most placed at $y = 1$ mm (still inside the domain). The order parameter is obtained after averaging over 50 independent realizations and over the last quarter of the simulation (150 min

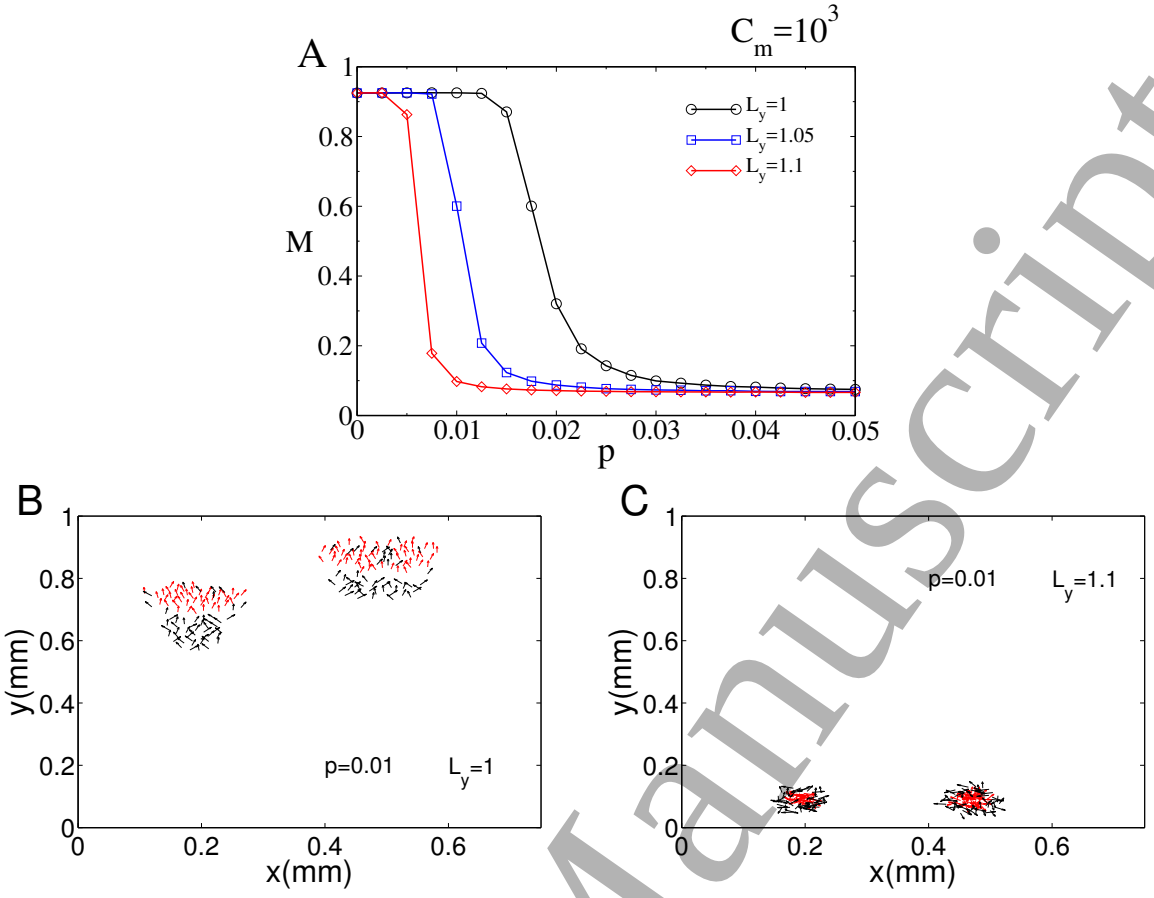

Figure 1. Behavior of the system as a function of the parameter p (in units of mm^{-3}), for different values of L_y (in units of mm). (A) Order parameter M as a function of p obtained after averaging over 50 independent realizations and over the last quarter of the simulation (150 min $< t <$ 200 min). (B) and (C) show spatial cell distribution on the domain at $t = 200$ min, with $p = 0.01$. We consider that each cell i belonging to the group A (black color) reacts to the chemical signals with a chemoattractive sensitivity of $\chi_i = \chi_i^A = 0.75$, while any cell i of the second group B (red color – or gray on black/white prints) possesses a stronger chemotactive sensitivity of $\chi_i = \chi_i^B = 1.5$. The total number of cells in the system is $N = 200$ (and thus $N_A = N_B = N/2$), and for the two cell subpopulations we have $\nu_o = 0.005$ mm min^{-1}, $m_{ij} = m_c = 1.575$, $\mu_E = 3$ min^{-1} and $\alpha_i = \alpha = 0.5\ \forall\ i, j$. For the chemical signals we use D=0.024 mm^2 min^{-1}. In all cases $L_x = 0.75$ mm. At $t = 0$ min the cells are placed at $y = 0$ and homogeneously distributed along the domain 0.01 mm $< x <$ 0.71 mm, pointing in the y direction. Note that C_m is in units of mm^{-2}.

$<$ t $<$ 200 min). The figure shows a transition between a state of high alignment in which $M \approx 0.9$ and a state in which $M \approx 0.1$ (random cell directionality). The critical value of p around which the transition occurs decreases with L_y. In order to shed some light on this behavior, we plot in Figs. 1(B) and (C) cell distributions on the x-y domain, at $t = 200$ min (the less chemotactic N_A cells are represented in black colors, while the strong chemotactic N_B cells are shown in red colors – or gray on black/white

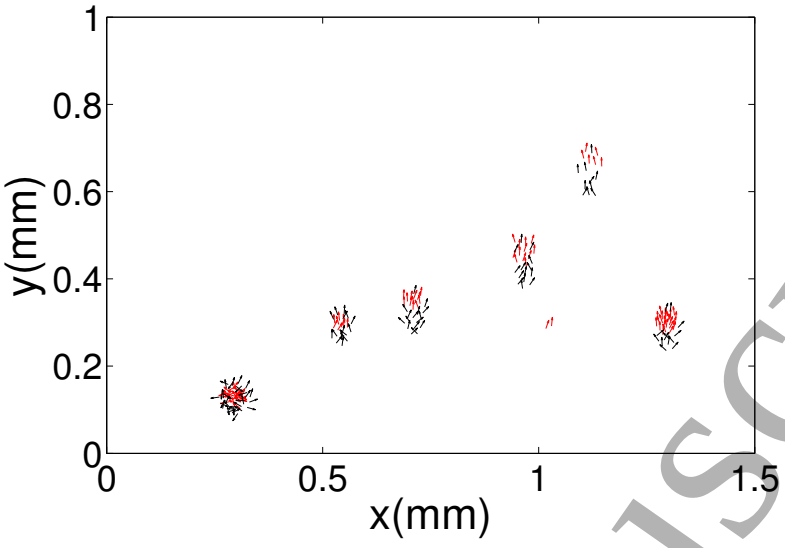

Figure 2. Spatial cell distribution on the domain at $t = 200$ min, with $L_x = 1.5$ mm and $L_y = 1.1$ mm. At $y = 0$ the cells are homogeneously distributed along the domain 0.01 mm $< x <$ 1.46 mm, pointing in the y direction. Other conditions and parameters are as in Figs. 2(B) and (C). The less chemotactic N_A cells are represented in black colors, while the strong chemotactic N_B cells are shown in red colors – or gray on black/white prints.

prints). All simulations start at $t = 0$ min with two hundred uniformly distributed cells placed at $y = 0$ and pointing along the y direction (not shown here). In panel (B) one observes that for $L_y = 1$ mm not only the formation of cell aggregations at different position in space occur, but also a complete spatial sorting of the two sub-populations of cells emerge (with the majority of the less chemotactic aggregates lagging behind the strong chemotactic ones). In panel (C) we see that slightly larger values of L_y lead to undirected and engulfed aggregates (the stronger chemotactic cells are engulfed by the less chemotactic ones). Thus, increasing the size of the domain along the y direction promotes the formation of undirected cell aggregations each of them containing both populations.

Figure 2 shows that the extension of the domain along the x direction (parameter L_x in our model) increases the number of cell aggregations. It also suggests that small and strong chemotactic cell aggregations move faster (we will come back to this point later). Note that in this case, simulation conditions and parameters are as in Fig. 1. From Figs. 1 and 2 one can conclude that, under our simulation conditions (i.e μ and D fixed), the larger the size of the domain the larger the number of undirected cell aggregations formed.

Now we proceed to study how the alignment of the cells is affected by the control parameters p, μ, and C_m. Figures 3(A) and (B) shows the order parameter M as a

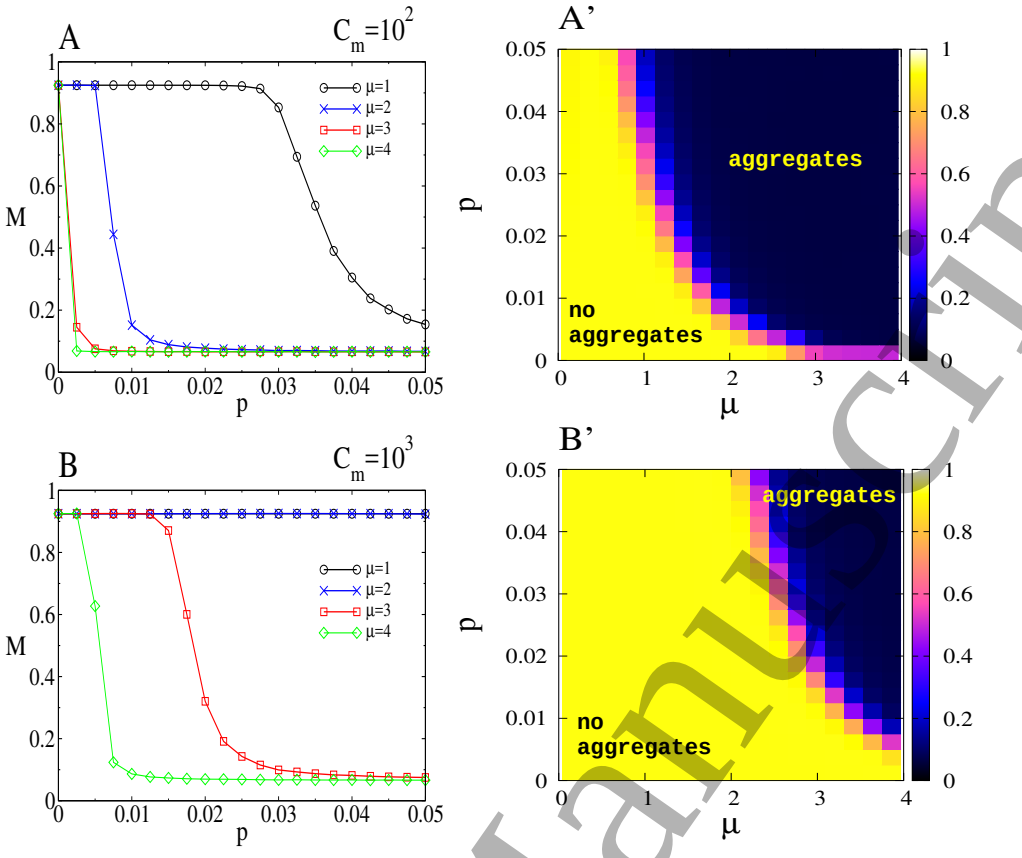

Figure 3. The order parameter M as a function of p (in units of mm^{-3}) and degradation rate μ (in units of min^{-1}), for two different external gradient steepness C_m in mm^{-2}. (A) and (B) show M as a function of p , for four different values of μ. (A') and (B') show the corresponding behavior of M in the phase plane (p,μ), for two values of C_m. We consider that each cell i belonging to the group A reacts to the chemical signal with a chemoattractive sensitivity of $\chi_i = \chi_i^A = 0.75$, while any cell i of the second group B possesses a stronger chemotactive sensitivity of $\chi_i = \chi_i^B = 1.5$. The total number of cells in the system is $N = 200$ (and thus $N_A = N_B = N/2$), and we have $\nu_o = 0.005$ mm min^{-1}, $\mu = 3$ s^{-1}, $m_{ij} = m_c = 1.575$ and $\alpha_i = \alpha = 0.5\ \forall\ i, j$. We consider a domain with $L_x = 0.75$ mm and $L_y = 1.0$ mm. For (A) and (B) M is obtained after averaging over 50 independent realizations and over the last quarter of the simulation (150 min $< t <$ 200 min). For (A') and (B') the average is obtained over 10 independent realizations. For the chemical signal we use D=0.024 mm^2 min^{-1}. At $t = 0$ min the cells are placed at $y = 0$, homogeneously distributed along the domain 0.01 mm $< x <$ 0.71 mm, and pointing in the y direction. **Note that aggregate formation was assessed by visual inspection.**

function of p, for several values of μ and C_m. These figures show that the critical value of p around which a transition occurs from an alignment state ($M \approx 0.9$) to an undirected state ($M < 0.2$) decreases with the degradation rate μ and increases with the steepness C_m of the external gradient. Figures 3(A') and (B') show the corresponding phase plane (p, μ) of M for $C_m = 10^2$ mm^{-2} and $C_m = 10^3$ mm^{-2}, respectively. These diagrams clearly show that, under our simulation conditions, the collective alignment

increases with C_m but decreases with p and μ. Typical examples of cluster distributions at $t = 200$ min for several values of p with $\mu = 2$ min^{-1} and $C_m = 10^2$ mm^{-2} are presented in Fig. 4. Figure 4(A) shows that for $p = 0.002$ mm^{-3} (inside the complete alignment zone of Fig. 3(A')) all cells move approximately in a straight line along the y direction and that the more chemotactic ones are the first to reach the upper wall. It also reveals the formation of weakly cohesive clusters. Figure 4(B) shows that for $p = 0.007$ mm^{-3} (around the transition zone between aligned and unaligned motion of Fig. 3(A')), two cell aggregations are formed, in which a partial sorting between the two subgroups of cells occurs, and the strong chemotactic cells start to overtake the less chemotactic ones. Finally, Figure 4(C) shows that for $p = 0.02$ mm^{-3} (i.e., inside the zone of undirected motion of Fig. 3(A')) two cell aggregations can form, where the strong chemotactic cells are engulfed by the less chemotactic ones. As noted in Fig. 3, a similar dynamics occurs if parameter p is fixed and one increases the degradation rate μ.

The spatial cell configurations presented above emerge from the interplay between the cell-cell attraction and the soft repulsion between cells. If the chemotactic attraction is small enough the cells tend to keep their initial orientation towards the y direction and the stronger chemotactic cells move most of the time in front of the less chemotactic ones (see video S2A in the supplementary material, and Fig. 4(A)). For moderate chemical attraction, it is common to observe the formation of cohesive cell aggregates. However, after an initial period of time, the strong chemotactic cells start to migrate to the front of the aggregates (see video S2B in the supplementary material, and Fig. 4(B)). For large chemo-attraction, one observes the formation of strongly cohesive cell aggregates with the stronger chemotactic cells collected in the middle. These aggregates move and interact trough the chemical signal produced by themselves. Eventually, they merge and form a single big aggregate (see video S2C in the supplementary material, and Fig. 4(C)).

We would like to emphasize that the merging process between aggregates is more frequent when the influence of the external chemical gradient is small. Under this condition, the aggregates have enough time to interact and merge. When the influence of the external gradient is large, the cells tend to move aligned towards the y directions and the aggregates do not have time to merge before reaching the upper wall of the domain. We note that the aggregates also merge when the size of the domain and/or the cell-cell attractive chemical interactions are large enough.

Figure 5(A) shows that for $C_m = 10^3$, the cells or the partially formed cell aggregates do not have time to merge before they reach the upper wall. However, by decreasing C_m to $C_m = 10^2$ as in Fig. 5(B), a single cell aggregate can emerge and remains inside the domain for very long time – shown here is $t = 400$ min. This single aggregate is the result of the collision between two separate aggregates due to the mutual chemical attraction (see the corresponding two aggregates in Fig. 4(C)).

One can associate the black and dark blue regions of Fig. 3 (A') and (B') with the formation of slow moving aggregates, the yellow regions with a more

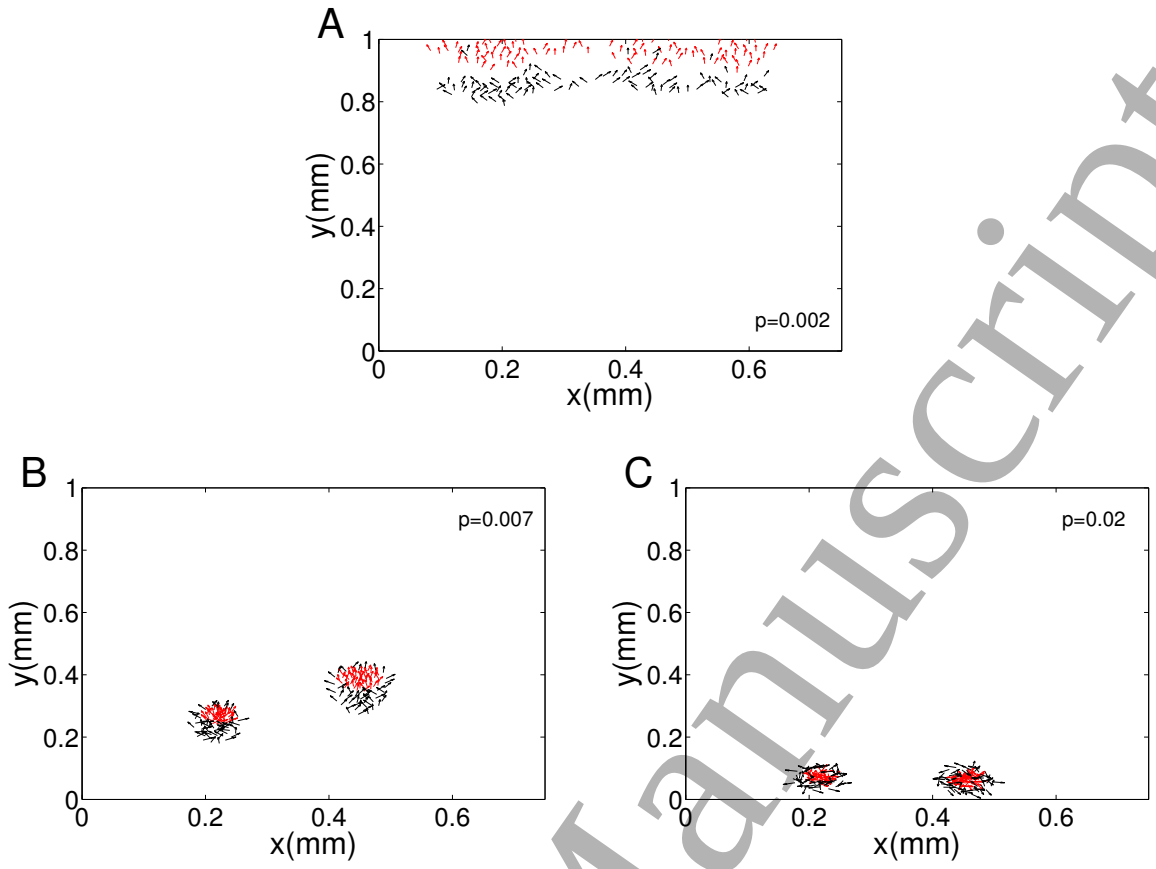

Figure 4. Spatial cell distribution at $t = 200$ min for three values of p (in units of mm^{-3}), with $\mu = 2$ min^{-1} and $C_m = 10^2$ mm^{-2} (corresponding to Fig. 3(A) and (A')). We consider that each cell i belonging to the group A (black color) reacts to the chemical signal with a chemoattractive sensitivity of $\chi_i = \chi_i^A = 0.75$, while any cell i of the second group B (red color – or gray on black/white prints) possesses a stronger chemoattractive sensitivity of $\chi_i = \chi_i^B = 1.5$. All other parameters are as in Fig. 3.

or less independent migration of the cells towards the external gradient, and the transition regions with the formation of aggregates that most of the time move as a whole towards the external gradient. Aggregate formation was assessed by visual inspection.

In the following section we explore the case in which the two sub-populations also differ in their average cell speeds.

3.2. Two groups of cells differing in cell speed and chemotactic sensitivity.

Taking into account the common assumption that strongly chemotactic cells move faster [6], we assume that each cell i belonging to the group A reacts to the chemical signal with a chemoattractive sensitivity of $\chi_i = \chi_i^A = 0.75$ and moves with a cell speed of $\nu_i^A = \nu_o^A + \epsilon g_i$, while any cell i of the second group B possesses a stronger chemoattractive sensitivity of $\chi_i = \chi_i^B = 1.5$ and moves with a higher cell speed of $\nu_i^B = \nu_o^B + \epsilon g_i$.

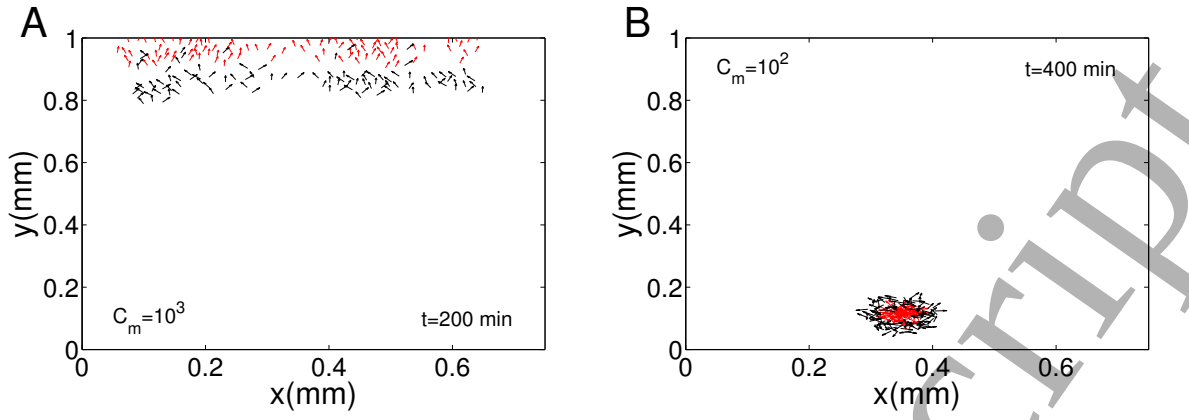

Figure 5. Spatial distribution of cells for two different C_m values. Here $p = 0.02$ mm^{-3}, and all other parameters are as in Fig. 4. The cells in subgroup A are shown in black color, and the cells in subgroup B are shown in red color – or gray on black/white prints.

Moreover, we assume that $\nu_o^A = 0.005$ mm min^{-1} and $\nu_o^B = 0.01$ mm min^{-1}. As before, $\epsilon = 10^{-4}$ mm min^{-1}, g_i is a nondimensional number drawn from a Gaussian distribution with zero mean and unit variance, $m_{ij} = m_c = 1.575$ and $\alpha_i = \alpha = 0.05 \; \forall \; i, j$. First, let us mention that the impact of the size of the domain and the parameters p, μ, and C_m on this new version of the model is similar to the one reported in previous section. Namely, the global alignment of cells decreases with the size of the domain along the y direction, the chemo-attraction between cells, and the chemical degradation rate, and increases with the steepness of the external chemical signal. Therefore, in the following we report only the major differences between the two cases (with similar or different cell speeds).

In Fig. 6 we plot separately the temporal evolution of the order parameter M for each subgroup normalized by the total number of cells (i.e., $0 \leq M \leq 0.5$, with $M = 0.5$ representing a totally aligned state inside each group). We choose to use values of p and μ inside the zone of complete alignment of Fig. 3(B) and (B'). Figures. 6(A), (B), and (C) show M as a function of time for the case in which the two groups differ in average speed and chemotactic sensitivity. The black solid curves describe the time evolution of M calculated for the slow and less chemotactic group of cells, while the dashed red curves describe the temporal behavior of M for the fast and highly chemotactic group of cells. Our simulations show that, in the long run, the two group of cells align almost totally. This is in agreement with Figs 3(B) and (B') of the previous section. The numerical simulations also show that there is a time interval during which the slow and less chemotactic group of cells exhibits a better alignment than the fast and stronger chemotactic group of cells. Interestingly, the period of time during which this phenomenon occurs increases with the number of cells in the system. However, as Figs. 6(D), (E), and (F) reveal, this phenomenon does not exist or it is not

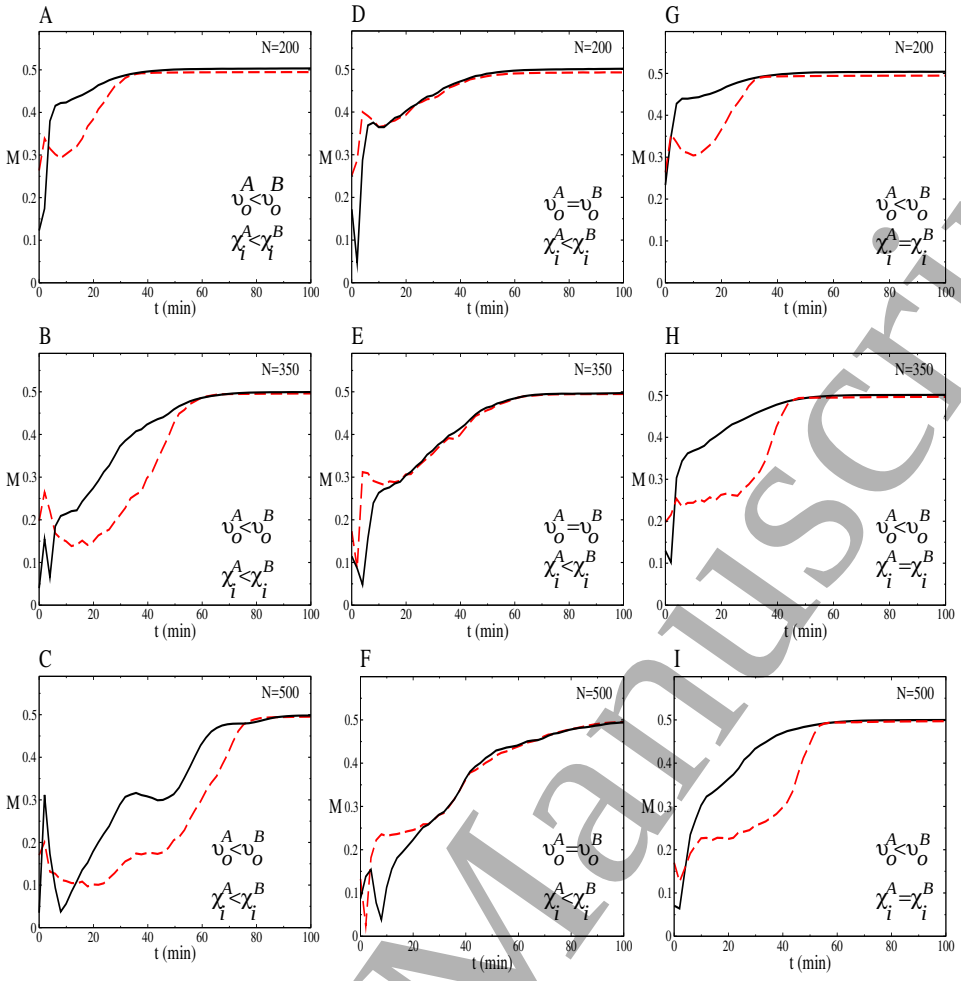

Figure 6. Temporal evolution of the order parameter M for three system sizes N. In panels A, B, C: $\chi_i^A < \chi_i^B$ and $v_o^A < v_o^B$, and we assume $\chi_i^A = 0.75$, $\chi_i^B = 1.5$, $\nu_o^A = 0.005$ mm min^{-1}, and $\nu_o^B = 0.01$ mm min^{-1}. In panels D, E, F: $\chi_i^A < \chi_i^B$ and $v_o^A = v_o^B$, and we use $\nu_o^A = \nu_o^B = 0.005$ mm min^{-1}, $\chi_i^A = 0.75$, and $\chi_i^B = 1.5$, In panels G, H, I: $\chi_i^A = \chi_i^B$ and $v_o^A < v_o^B$, and we consider $\chi_i^A = \chi_i^B = 1.5$, $\nu_o^A = 0.005$ mm min^{-1}, and $\nu_o^B = 0.01$ mm min^{-1}. In all cases the subgroup with $N_A = N/2$ cells is described by black curves, while the subgroup with $N_B = N_A$ cells is described by red dashed curves. In all cases $\mu = 2.0$ min^{-1}, $p = 0.04$ mm^{-3}, $C_m = 10^3$ mm^{-2}, $\alpha_i = \alpha = 0.05$, and $m_{ij} = m_c = 1.575\ \forall\ i, j$. For the domain size we use $L_x = 0.75$ mm and $L_y = 1$ mm. All curves are obtained after averaging over 50 independent realizations. For these plots we show only the time $t \in [0.02, 100]$min.

significant when the two groups differ only in their chemotactic sensitivity. In this case, after a short time the two groups exhibit almost the same alignment. Figures 6(G), (H), and (i) show that this interesting phenomenon occurs even when the two groups have the same chemotactic sensitivity, but differ in their average cell speed. In both cases, the duration of the migrating phenomenon increases with the number of cells in the system. In Fig. 7, we show the spatial cell distribution of $N = 500$ cells, for the case in which the two groups differ in their average cell speed and their chemical

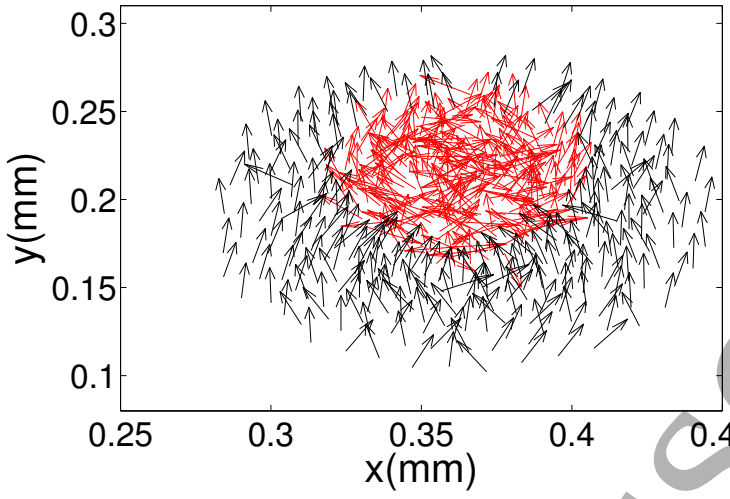

Figure 7. Detailed description of the spatial distribution of cells on the domain, when $N = 500$ and time $t = 70$ min. Here we show the case in which the two groups differ in velocity and chemical sensitivity (corresponding to Fig. 6(C)). In this case the black arrows represent slow and less chemotactic cells, while the red arrows represent fast and highly chemotactic ones.

sensitivities (corresponding to Fig. 6(C)). It shows that at $t = 70$ min the fast and stronger chemotactic red (gray on black/white prints) cells collect in the middle of the aggregates, with their velocity vector pointing in random directions. In contrast, the slow and less chemotactic black cells move aligned towards the aggregate formed by the inner cells or/and the external chemical gradient (see videos S3 in the supplementary material, for a better understanding of the corresponding cell distribution patterns). Finally, we would like to emphasize that for all these plots the time runs from 0.02 min to 100 min. This is the reason why the initial state in which $M = 1$ does not appear in these simulations.

We also analyze the impact of the noise parameter α on the cell migrating phenomenon presented above. Figure 8 shows the temporal evolution of M for three different noise intensities, when $N = 500$. Note that the time interval during which this phenomenon occurs increases with the noise intensity. This is due to the fact that the noise delays the time for cells to reach a completely aligned state, as induced by the external chemical gradient. These results also reveal that, as expected, the difference in the levels of alignment between the two groups decreases with the noise intensity.

In the following section we explore the changes in the speed of cell aggregations as a function of some model parameters.

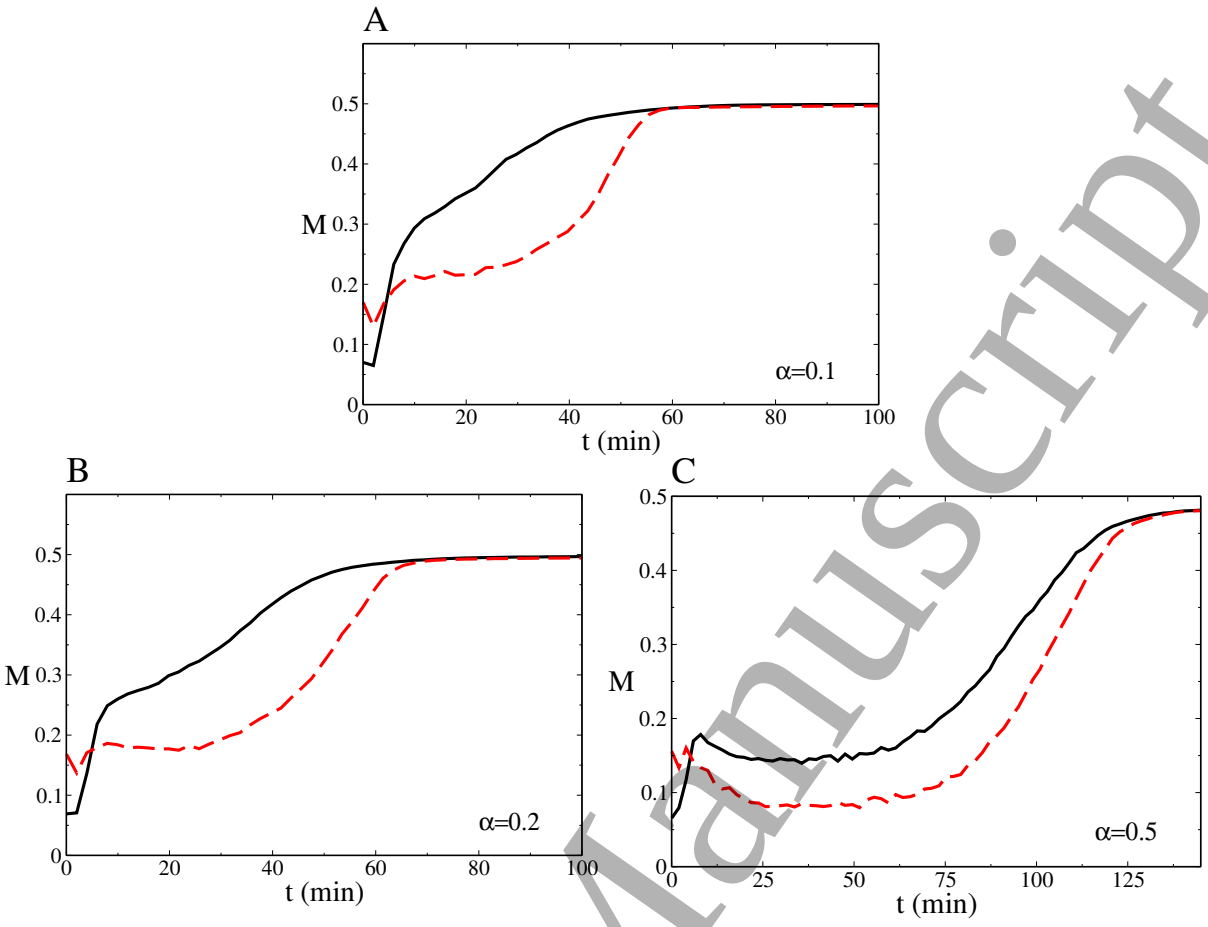

Figure 8. Temporal evolution of the order parameter M for three noise intensities α, with $N = 500$. Parameters are as in Fig. 6(I). Again, for these plots we show only time $t \in [0.02, 100]$min. All curves are obtained after averaging over 50 independent realizations.

3.3. Speed of cell aggregations as a function of control parameters.

In this section we explore the speed of single aggregates as a function of the number of cells (N) and some other parameters of the system (e.g., p, μ, L_y). For simplicity, we assume that all cells have the same average speed ($\nu_o^A = \nu_o^B = \nu_o$) and chemical sensitivity ($\chi_i^A = \chi_i^B = \chi$, for all i). We pay attention to the velocity component along the y direction of a single aggregate (V_y). To calculate this velocity, we identify the center of the aggregate and measure the displacement of this central point during the last quarter of the simulation (150 min $< t <$ 200 min). We assume that initially, cells are homogeneously distributed in a small sub-domain, with all of them pointing in the y direction. We denote the number of cells in the aggregate by N (since for these simulations all cells in the population form an aggregate). In the supplementary material we show examples of some aggregates used to calculate the speed (e.g., see video S4 for an illustration of how these aggregates move over time and space).

In Fig. 9 we plot V_y as a function of the cluster size N, for several values of p, μ, and

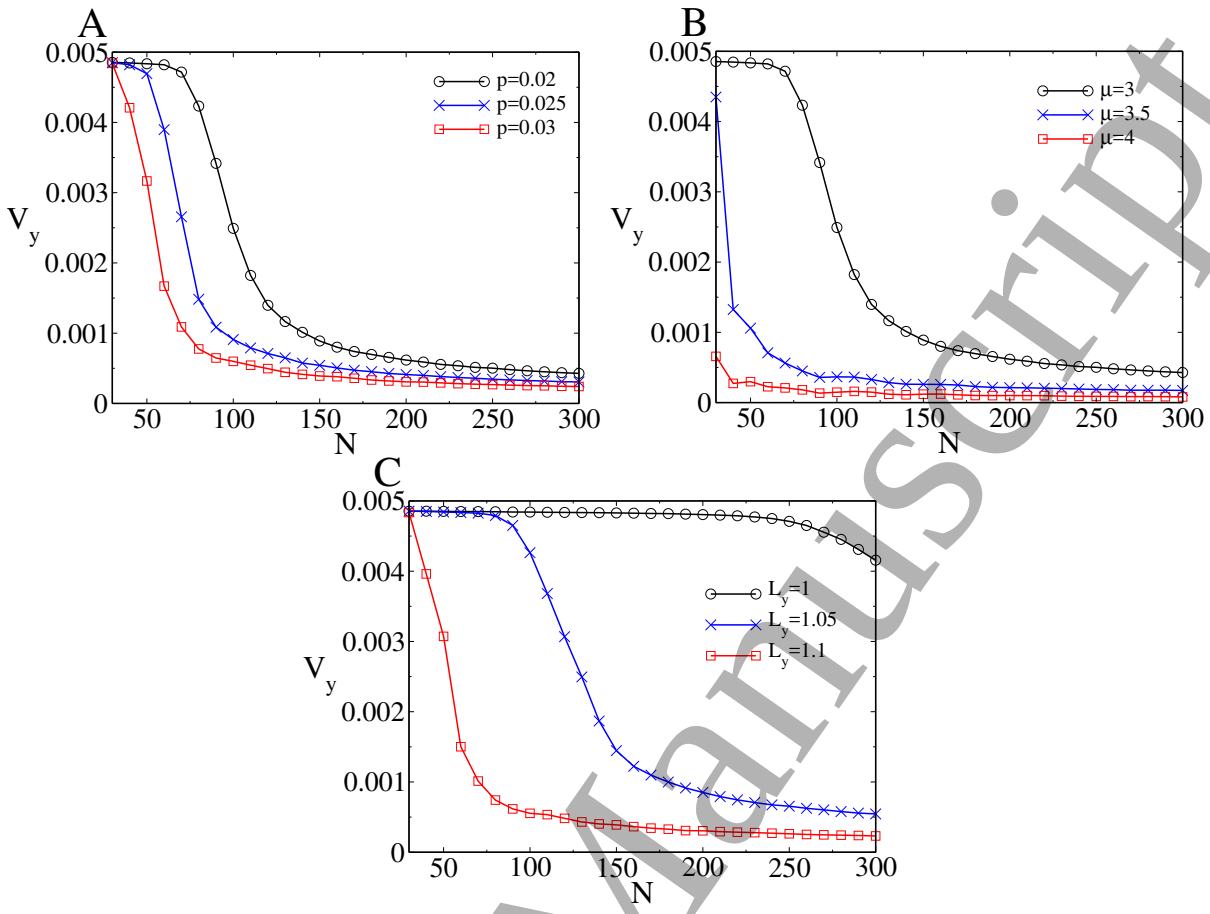

Figure 9. Magnitude of the velocity component along the y direction (V_y) of a single aggregate, as a function of the population size N. (A) V_y versus N for three different values of p in units of mm^{-3}, with $\mu = 3$ min^{-1}. (B) V_y versus N for three different values of μ in units of min^{-1}, with $p = 0.02$ mm^{-3}. In (A) and (B) the size of the domain is given by $L_x = 0.6$ mm and $L_y = 1.0$ mm. (C) V_y versus N for three different values of L_y in units of mm, with $\mu = 3$ min^{-1}, $p = 0.01$ mm^{-3} and $L_x = 0.6$ mm. For all cases we consider that $\nu_o = 0.005$ mm min^{-1}, $\chi_i = \chi = 1.5$, $C_m = 10^3$ mm^{-2}, $\alpha_i = \alpha = 0.5$, $m_{ij} = m_c = 1.575$ $\forall$ i, j. The velocity is obtained after averaging over 50 independent realizations.

L_y. The figure shows that the velocity along the y direction decreases with the number of cells (since the attraction towards the center of the aggregate due to local chemical signals increases with the increase in cell numbers). Panels (A), (B), and (C) also show that such velocity decreases with the response of the cell to the chemical signal secreted by themselves (parameter p), the chemical degradation rate μ, and the extension of the domain along the y direction, L_y. Moreover, Fig. 10 shows that V_y increases with the chemotactic sensitivity of cells. Also in this case, the speed decreases with p and μ. These results explain why, in the case of two different subpopulations, the smaller and stronger chemotactic aggregates move faster (see for instance Fig. 2).

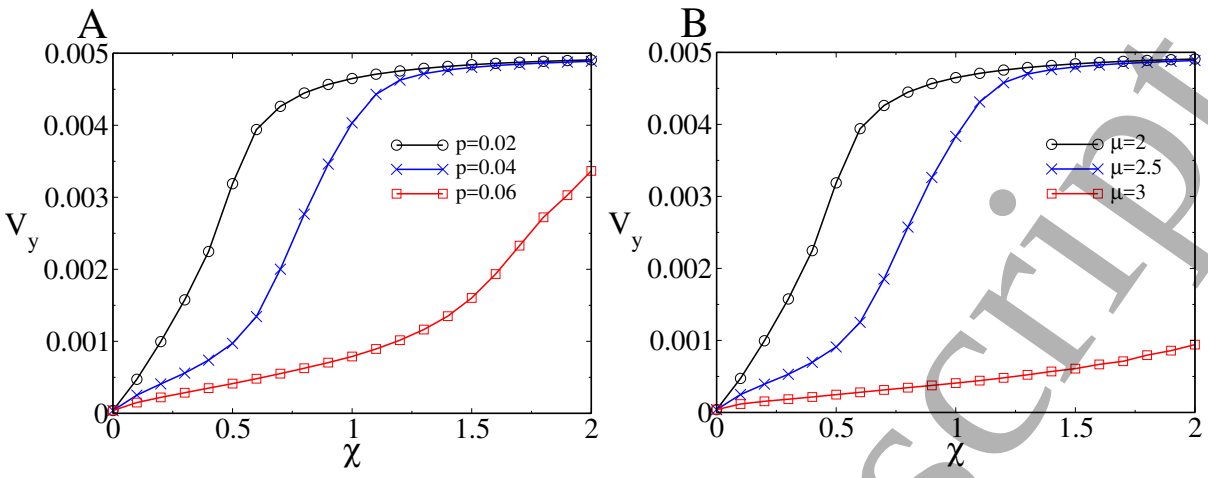

Figure 10. Magnitude of the velocity component along the y direction (V_y) of a single aggregate, as a function of the chemical sensitivity χ. (A) V_y versus χ for three different values of p in units of mm^{-3}, $\mu = 2$ min^{-1}. (B) V_y versus χ for three different values of μ in units of min^{-1}, with $p = 0.02$ mm^{-3}. We consider that for both cases, $\nu_o = 0.005$ mm min^{-1}, $N = 200$, $C_m = 10^3$ mm^{-2}, $\alpha_i = \alpha = 0.5$, and $m_{ij} = m_c = 1.575$ $\forall$ i, j. The velocity is obtained after averaging over 50 independent realizations. For the size of the domain we use $L_x = 0.6$ mm and $L_y = 1.0$ mm.

4. Summary and Discussion

In this work, we generalized a one-population self-propelled particle system introduced in [15] to further describe systematically the dynamics of populations of distinct heterogeneous cells, and then used it to assess the chemotactic response of the cells to imposed stationary chemical gradients. First, we considered two cell populations that differ in their chemotactic sensitivity. Then, we analyzed the case in which the two populations also differ in their average cell speed. We found that the response of the two populations to the external chemical gradient was strongly affected by the response to the chemical signal secreted by the cells themselves and the chemical signal degradation rate. Our simulations also revealed that the size of the domain inside which the cells migrate, the number of cells in the domain, and the intrinsic random motion of the cells played an important role on the collective migration. Beside the investigation of cell alignment (via changes in the order parameter M), we also investigated the formation of cell aggregations, and how the speed of single aggregates was affected by the main control parameters of the model.

The case when the two cell populations differ only in their chemotactic sensitivity predicted a number of interesting phenomena. First, we found that the size of the domain determined the number of cell aggregations formed in response to the cell-cell chemical attraction (see Figs. 1 and 2). If the initial distribution of cells was homogeneous along the x direction of the domain, then the larger the size of the domain the larger the number of cell aggregations observed. Moreover, increasing the length of the domain

along the y direction induced slow moving cell aggregations, with cells inside them exhibiting undirected motion. All this behaviour occurred in part due to the exponential decrement of the external chemical signal near the upper wall of the domain, and the dominance of the chemical signal secreted by the cells themselves.

We also found that the collective alignment of cells decreased with: the size of the domain along the y direction, the response of the cells to the chemical signal generated by themselves, and the chemical signal degradation rate (see Figs. 1 and 3). Our simulations also showed that small steepness of the external chemical gradient favours the formation of cell aggregates and the undirected motion of cells, while large gradient steepness induced complete cell alignment (see Fig. 3). Moreover, the simulations commonly showed the formation of cell aggregates in which the fast moving cells were engulfed or partially engulfed by the slow moving ones. In addition, a number of completely segregated cellular aggregations were also observed (see, for instance, Figs. 1(B), 2, and 4, and the videos in the supplementary material). We also found that the merging process between cell aggregates was more pronounced when the influence of the external gradient was not too strong to counteract the chemical aggregate-aggregate attraction (see Fig. 5).

Although not discussed in detail, we also found that the phenomena mentioned above occurred in the situation where the two subpopulations of cells simultaneously had different chemotactic sensitivities and cell speeds (see Fig. 6 for an example of complete alignment that both versions of the model exhibited in the long run). However, in this work we only payed attention to the main difference between the two aforementioned cases. We found that when the two groups differ in cell speeds and chemotactic sensitivities, there was an initial-to-intermediate period of time during which the slow moving cells exhibited a better alignment than the fast moving ones (see Fig. 6). This behaviour, which was not observed when the subpopulations differ only in chemotactic sensitivity, was mainly due to the differences in cell speed between the two subgroups of cells. We also found that the intrinsic noisy behaviors of cells lead to an increment in the time interval during which this phenomenon was observed. However, the noise also decreased the difference in alignment between the two subpopulations (see Fig. 8).

Finally, we analyzed the speed of a cell aggregate as a function of the main control parameters of the model. For simplicity, we assumed that all cells possessed the same average speed and chemotactic sensitivity. We generated a single aggregate and measured the velocity of it while moving along the y direction towards the external chemical gradient. We found that the velocity decreased with: the number of cells, the response of the cells to the local chemical signal generated by themselves, the chemical degradation rate, and the extension of the domain along the y direction (see Fig. 9). Our simulations also showed that the speed of aggregates increased with the chemotactic sensitivity of cells χ (see Fig. 10). These results allow us to conclude that, in our model, smaller and highly chemotactic cell aggregates move faster compared to larger or weaker chemotactic aggregates.

The model has a number of experimentally relevant parameters (e.g., N, p, μ, ...),

which allowed us study numerically, in a simple but general way, the collective migration of heterogeneous cell populations. This study was motivated by the experimental results reported by Guven *et. al.* [15], which investigated the response of a single homogeneous population of cells to external chemical linear gradients and signal relay. Thus, in principle, we expect that some of the phenomena reported in our study also occur in experiments performed with subpopulation of cells having different chemotactic properties and/or cell speeds (see, for example, the chemotactic cell sorting reported in [1] for a heterogeneous population of skin fibroblasts and malignant fibrosarcoma cells). We also need to emphasize that our model does not take into account the exact experimental conditions implemented by Guven *et. al.* [15]. In that experimental study the authors injected a uniform flux of cells, in which any newly introduced cell was oriented more or less in the y-direction. Thus, the number of cells in their experimental setup increased in time, which is in contrast to our theoretical model where we assumed a finite number of cells at the initial time. Furthermore, in Guven *et. al.* [15], once the cells reached the upper wall of the domain, they were removed from the experiment. That experiment also considered that the external chemical gradient is a linear one, whereas in our theoretical model the gradient normally exhibits an exponential decay. All these differences could be included in our minimalistic model. We will explore these aspects in our future research.

Although the model investigated in this study predicted interesting and potentially verifiable collective phenomena in heterogeneous cell populations (as is the segregation of stronger/weaker chemotactic cells in [1]), it could be further extended in several different ways. Two such approaches, which focus on the incorporation of saturated cell chemotactic responses to large concentrations of chemicals (as observed experimentally [13]), and on the incorporation of cell-cell adhesive forces (which have been shown to affect cell aggregation and sorting [5, 39]), are also the topic of on-going work. **Instead of considering two single subpopulations of cells, it could be also interesting to assume that each cell has a different response to the chemical signals. These type of cell-to-cell variations were recently included in a model of collective chemotaxis, and it was found that chemotaxis is limited by cell-to-cell variation in signaling [40]**. While our study focuses on a simple model, our numerical results could help advance the understanding of the complex and orchestrated movement of heterogeneous cell populations toward external chemical signals.

Acknowledgments

MP and RE acknowledge partial support from a previous Engineering and Physical Sciences Research Council (UK) grant number EP/K033689/1.

Supporting Information

S1 Figure. **External chemical profile as described by Eq. (6)**. (A) Profile as a function of L_y in units of mm, with $\mu_E = 3$ min^{-1}. (B) Profile as a function of μ_E in units of min^{-1}, with $L_y = 3$ mm. In both plots D_E=0.024 mm^2 min^{-1}. Note that C_E is in units of mm^{-2}.

S2 Video. **Temporal evolution of cells for two subpopulations with different chemotactic sensitivities (corresponding to Fig. 4).** (A) In this case $p = 0.002$ mm^{-3}. The system forms some weakly cohesive aggregates, where the majority of strong chemotactic cells are moving in front of the less chemotactic ones. (B) In this case $p = 0.007$ mm^{-3}. Initially three aggregates emerge, with the strong chemotactic cells collecting in the middle of the aggregates. At this time all cells are oriented randomly. As time progresses, two of the aggregates start merging. Eventually, due to the chemotactic attraction towards the external chemical gradient, the cells align in the y direction. The strong chemotactic cells move to the front of the aggregates. (C) In this case $p = 0.02$ mm^{-3}. As in (B), we first observe the formation of three aggregates, where the strong chemotactic cells are collected in the middle of the aggregates. As time progresses, aggregates start merging until they form a single, very slow moving aggregate formed of stronger chemotactic cells in the middle (depicted in red; or gray on black/white prints), and weaker chemotactic cells at the exterior (depicted in black). The arrows are scaled to avoid overlapping when many cells are close to each other. They give the direction of the cell's velocity but not its magnitude.

S3 Video. **Temporal evolution of cells for two subpopulations.** (A) Two subpopulations that differ in cell speed and chemotactic sensitivity (corresponding to Fig. 6(C) in main text). After an initial transient behavior, the faster and stronger chemotactic cells depicted in red (gray on black/white prints) are engulfed by the slower moving and less chemotactic ones. These faster cells exhibit poor alignment in comparison with the slower moving cells. Towards the end of the simulations, both types of cells become aligned in the y direction, and the faster ones start to overtake the others. The less chemotactic cells align towards the external chemical signal or towards the big cluster of faster moving cells. (B) Two subpopulations with different chemotactic sensitivities but equal cell speeds (corresponding to Fig. 6(F) in main text). After an initial transient behaviour, all cells merge into one single aggregate with the inside cells (and the outside cells) aligned towards the y direction. (C) Two subpopulations differing only in cell speeds (corresponding to Fig. 6(I) in main text). Two aggregates form very quickly, with the faster cells at the front of these moving aggregates. Eventually the faster cells split from the slower cells. The total number of cells is $N = 500$. The arrows are scaled to avoid overlapping when many cells are close to each other. They give the direction of the cell's velocity but not its magnitude.

S4 Video. **Temporal evolution of a single homogeneous aggregate.** In this case all cells have the same average speed and chemotactic sensitivity. (A) An aggregate

containing 50 cells. The aggregate is not rigid but expands while moving to the y direction (towards the maximum of the external chemical gradient). (B) An aggregate containing 200 cells. In this case, the aggregate is little more compact, but move very slow in comparison with the case presented in (A). We consider $p = 0.02$ mm^{-3}, $\mu = 3.0$ min^{-1}, $N = 50$, and $C_m = 10^3$ mm^{-2}. We also consider that for all cells $\nu_o = 0.005$ mm min^{-1}, $\chi_i = \chi = 1.5$, $\alpha_i = \alpha = 0.5$, $m_{ij} = m_c = 1.575\ \forall\ i, j$. For the size of the domain we use $L_x = 0.6$ mm and $L_y = 1.0$ mm. Initially the cells are homogeneously distributed inside a domain located in $0 < y < 0.05$mm and $0.25 < x < 0.35$mm, and pointing in the y direction. The arrows are scaled to avoid overlapping when many cells are close to each other. They give the direction of the cell's velocity but not its magnitude.

S5 Code. Code and documentation to run our simulations is provided in the file PinedaEftimieCode.

References

[1] Albini A, Müller PK, Parodi S 1984 *Bioscience Reports* **4** 311-318.
[2] Friedl P and Gilmour D 2009 *Nature Reviews, Molecular Cell Biology* **10** 445-457.
[3] Rørth P 2009 *Annu. Rev. Cell Dev. Biol* **25** 407-429.
[4] Dormann D and Weijer CJ 2003 *Curr. Opin. Genet. Dev* **13** 358-364.
[5] Duguay D, Foty RA, Steinberg MS 2003 *Dev. Biol.* **253** 309-323.
[6] Vasiev B and Weijer CJ 1990 *Biophys. J* **76** 595-605.
[7] Murray JD 2007 (*Springer, New York*).
[8] Dallon JC and HG Othmer HG 2004 *J. Theor. Biol* **231** 203-222.
[9] Woods ML, Carmona-Fontaine C, Barnes CP, Cousin ID, Mayor R, Page KM 2014 *PLoS ONE* **9** e104969. doi:10.1371/journal.pone.0104969.
[10] McLennan R, Dyson L, Prather KW, Morrison JA, Baker RE, Maini PK and Kulesa PM 2012 *Development* **139** 2935-2944.
[11] McLennan R, Schumacher lJ, Morrison JA, Teddy JM, Dennis A. Ridenour DA, Box AC, Semerad CL, Li H, McDowell W, Kay D, Maini PK, Ruth E. Baker RE and Kulesa PM 2015 *Development* **142** 2014-2025.
[12] Bretschneider T, Othmer HG and Weijer CJ 2016 *Interface Focus* **6** 20160047.
[13] Song L, Nadkarnia SM, Bödeker HU, Beta C, Bae A, Franck C, Rappel W-J, Loomis WF and Bodenschatz E 2006 *Eur J Cell Biol* **85** 981-989.
[14] Amselem G, Theves M, Bae A, Bodenschatz E and Beta C 2012 *PLoS ONE* **7** e37213. doi:10.1371/journal.pone.0037213.
[15] Guven C, Rericha E, Ott E and Losert W 2013 *PLoS Comput Biol* **9** e1003041. doi:10.1371/journal.pcbi.1003041.
[16] Lin F, Saadi W, Rhee SW, Wang SJ, Mittal S and Jeon NL 2004 *Lab. Chip* **4** 164-167.
[17] Wang SJ, Saadi W, Lin F, Nguyen CMC and Jeon NL 2004 *Exp. Cell Res* **300** 180-189.
[18] Thar R and Kuhl M 2003 *Proc. Natl. Acad. Sci. USA* **100** 5748-5753.
[19] Cumming BD, McElwain DLS and Upton Z 2010 *J. R. Soc. Interface* **7** 19-34.
[20] Friedl P and Wolf K 2003 *Nature Reviews Cancer* **3** 362-374.
[21] Youk H and Lim WA 2014 *Science* **343** 1242782.
[22] Mehes E and Vicsek T 2014 *Integr. Biol* **6** 831.
[23] Vicsek T and Zafeiris A 2012 *Physics Report* **517** 71.
[24] Painter KJ 2009 *Bull. Math. Biophys* **71** 1117-1147.
[25] Painter KJ and Sherratt JA 2003 *J. Theor. Biol* **225** 327-339.

[26] **Foty RA and Steinberg MS** 2004 *Int. J. Dev. Biol* **48** 397-409.
[27] **Duguay D, Foty RA and Steinberg MS** 2003 *Dev. Biol* **253** 309-323
[28] McCann CP, Kriebel PW, Parent CA and Wolfgang LW 2010 *J. Cell. Sci* **123** 1724.
[29] Calovi DS, Brunnet LG and de Almeida MC 2010 *Phys. Rev. E* **82** 011909.
[30] Meyer M, Schimansky-Geier L and Romanczuk P 2014 *Phys. Rev. E* **89** 022711.
[31] Taktikos J, Zaburdaev V and Stark H 2011 *Phys. Rev. E* **84** 041924.
[32] Tindall MJ, Maini PK, Porter SL and Armitage JP 2008 *Bull. Math. Biol* **70** 1570.
[33] Camley BA, Zimmermann J, Levine H, and Rappel WJ 2016 *PLoS Comput Biol* **12**: e1005008. doi:10.1371/journal.pcbi.1005008.
[34] Henkes S, Fily Y and Marchetti MC 2011 *Phys. Rev. E* **84** 040301(R).
[35] Garcia T, Brunnet LG and Silvia De Monte S 2014 *PLoS Comput Biol* **10** e1003482. doi:10.1371/journal.pcbi.1003482 .
[36] Vicsek T, Czirók A, Ben-Jacob E, Cohen I and Shochet O 1995 *Phys. Rev. Lett* **75** 1226.
[37] Coburn L, Cerone L, Torney C and Couzin ID 2013 *Phys. Biol* **10** 046002.
[38] Tunstrøm K, Katz Y, Ioannou CC, Huepe C, Lutz MJ and Couzin ID. 2013 PLoS Comput Biol **9** e1002915. doi:10.1371/journal.pcbi.1002915
[39] Belmonte JM, Thomas GL, Brunnet LG, de Almeida RMC and Chaté H. 2008 *Phys. Rev. Lett* **100** 248702.
[40] **Camley BA and Rappel W-J** 2017 arXiv:1707.03532.